The EMBO Journal Vol. 20 No. 3 pp. 340–349, 2001

The extracellular human melanoma inhibitory activity (MIA) protein adopts an SH3 domain-like fold

Raphael Stoll, Christian Renner, Markus Zweckstetter, Michael Brüggert, Dorothee Ambrosius[1], Stefan Palme[1], Richard A.Engh[1], Michaela Golob[2], Ines Breibach[2], Reinhard Buettner[2], Wolfgang Voelter[3], Tad A.Holak[4] and Anja-Katrin Bosserhoff[2,4]

Max Planck Institute of Biochemistry, D-82152 München, [1]Roche Diagnostics GmbH, Pharmaceutical Research, D-82377 Penzberg, [2]University Hospital of RWTH Aachen, Institute of Pathology, D-52074 Aachen and [3]Tübingen University, Department of Physical Biochemistry, Institute of Physiological Chemistry, D-72076 Tübingen, Germany

[4]Corresponding authors
e-mail: holak@biochem.mpg.de or bosserhoff@pat.rwth-aachen.de

Melanoma inhibitory activity (MIA) protein is a clinically valuable marker in patients with malignant melanoma, as enhanced values diagnose metastatic melanoma stages III and IV. Here we show that the recombinant human MIA adopts an SH3 domain-like fold in solution, with two perpendicular, antiparallel, three- and five-stranded β-sheets. In contrast to known structures with the SH3 domain fold, MIA is a single-domain protein, and contains an additional antiparallel β-sheet and two disulfide bonds. MIA is also the first extracellular protein found to have the SH3 domain-like fold. Furthermore, we show that MIA interacts with fibronectin and that the peptide ligands identified for MIA exhibit a matching sequence to type III human fibronectin repeats, especially to FN14, which is close to an integrin $\alpha_4\beta_1$ binding site. The present study, therefore, may explain the role of MIA in metastasis *in vivo*, and supports a model in which the binding of human MIA to type III repeats of fibronectin competes with integrin binding, thus detaching cells from the extracellular matrix.

Keywords: extracellular SH3 domain/fibronectin/melanoma/MIA/NMR

Introduction

Melanoma progression and tumor growth are regulated by a complex network of paracrine and autocrine positive and negative growth factors (Bogdahn *et al*., 1989). The melanoma inhibitory activity (MIA) protein was identified within growth-inhibiting activities purified from the tissue culture supernatant of the human melanoma cell line HTZ-19. (Blesch *et al*., 1994). MIA is translated as a 131 amino acid precursor molecule and processed into a mature 107 amino acid protein after cleavage of a putative secretion signal (Blesch *et al*., 1994). MIA provides a clinically useful parameter in patients with metastatic melanoma stages III and IV (Bosserhoff *et al*., 1997, 1998; Deichmann *et al*., 1999; Dréau *et al*., 1999). MIA mRNA was identified independently by differential display approaches comparing melanoma cell lines, and also by comparing differentiated and dedifferentiated cartilage cells *in vitro*. Therefore, MIA has also been referred to as the cartilage-derived retinoic acid-sensitive protein (CD-RAP) (Dietz and Sandell, 1996). Subsequent studies of murine embryos and murine adult tissues have demonstrated specific mRNA expression patterns in cartilage, but not in any other non-neoplastic tissue. Thus, MIA might also be a potential serum marker for rheumatoid arthritis and cartilage damage (Müller-Ladner *et al*., 1999). MIA was described as having antitumor activity by inhibiting proliferation of melanoma cell lines *in vitro* (Bogdahn *et al*., 1989; Blesch *et al*., 1994). However, further studies have revealed expression patterns inconsistent with a tumor suppressor. Expression of the wild-type MIA protein gene was not detected in normal skin and melanocytes but was associated with progression of melanocytic tumors (Van Groningen *et al*. 1995; Bosserhoff *et al*., 1997). More recently, it was suggested that the MIA protein specifically inhibits attachment of melanoma cells to fibronectin and laminin, thereby masking the binding site of integrins to these extracellular matrix (ECM) components, and promoting invasion and metastasis *in vivo* (Bosserhoff *et al*., 1998, 1999). Thus, the growth-inhibitory activity *in vitro* would reflect the ability of the protein to interfere with the attachment of cell lines to culture dishes *in vitro* (Blesch *et al*., 1994). In the present paper, we report the three-dimensional (3D) structure of recombinant human MIA in solution, determined by multi-dimensional NMR spectroscopy. Furthermore, we discuss the dynamic properties of MIA in solution based on ^{15}N-T_2, ^{15}N{^{1}H}-NOE and ^{15}N(dipole-CSA) cross-correlation rate experiments. Finally, a model is proposed for the physiological function of human MIA based on the solution structure and biochemical interaction studies.

Results

Secondary structure of MIA and sequence-specific assignment of ^{1}H, ^{15}N and ^{13}C resonances

The dispersion of $^1H^N$-^{15}N HSQC (heteronuclear single-quantum correlation) resonances clearly indicates a folded protein, in agreement with bioassays performed with refolded recombinant MIA (Stoll *et al*., 2000).

Cysteine bonds are formed between Cys13 and Cys18, and Cys36 and Cys107, as could be shown by proteolytic digest, N-terminal amino acid sequencing and Ellman assay using bis-(4-nitrophenyl)-disulfide-3,3′-dicarbonic acid (data not shown). No unambiguous NOE patterns between β-β methylene groups for these residues could be

observed because of spectral overlap (Klaus *et al*., 1993). Nonetheless, structures including these disulfide bonds perfectly fulfill all experimental constraints used in the structure calculation of human MIA (see Discussion).

Secondary structure elements of human MIA were identified on the basis of characteristic sequential and medium range NOE patterns (Wüthrich, 1986). In addition, exchange of amide protons, values of the $^3J_{H\alpha HN}$ coupling constants and chemical shift indices were considered (Wüthrich, 1986; Wishart *et al*., 1991). Based on these criteria, the following eight antiparallel β-strands have been identified in MIA: βnt/ct, Arg10–Cys13/Val96–Lys99; βc/d, Gly62–Ser64/Leu77–Tyr79; βa/b, Ser23–Ala27/Gln45–Val49; βa/e, Ala25–Ala27/Val85–Glu87; βnt/b′, Arg10–Leu12/Lys52–Lys54; βb′/c, Ser51–Lys52/Trp61–Gly62; and β_{irr}, Asp30–Met32/Thr40–His42. These form two perpendicular, antiparallel, three- and five-stranded β-sheets: βct/βnt/βb′/βc/βd and βb/βa/βe. β_{irr} is an irregular short antiparallel β-sheet where only the central amino acids Tyr31 and Ile41 fulfill the ideal β-sheet geometry.

Tertiary structure of MIA

The structure of human MIA was calculated with a total of 1139 approximate inter-residue distance constraints derived from NOESY (nuclear Overhauser and exchange spectroscopy) spectra, supplemented with 22 dihedrals and 12 hydrogen bond constraints (Table I). The global fold is uniquely defined due to the large number of non-redundant NOEs (Figure 1). A total of 20 structures were calculated by a simulated annealing protocol implemented in the programme X-PLOR (Brünger, 1993). All structures satisfy the experimental constraints with small deviations from idealized covalent geometry and the average root mean square deviations (r.m.s.ds) from the mean structure (Table I). In general, the conformations of side chains are also well defined (data not shown). Ninety-eight percent of the backbone torsion angles lie within allowed regions of the Ramachandran plot, except for the few non-glycine residues outside these regions located at the structural interfaces of β-sheets and connecting loops. Figure 1 shows an ensemble <SA> of 20 structures of human MIA. In Figure 2, a ribbon diagram of the minimized average structure $(SA)_m$ computed from <SA> is presented. A DALI search identified a similarity of the structural fold of MIA to the SH3 domain of ABL tyrosine kinase, which is superimposed in Figure 2 (Holm and Sander, 1993).

Table I. Structural statistics of <SA>[a] for rhMIA in solution at 300 K and pH 7.0

Restraints for structure calculations	
Total restraints used	1139
Total NOE restraints	1117
intraresidue	355
sequential	343
medium range	128
long range	279
hydrogen bond restraints	12
Statistic for structure calculations	<SA>[a]
R.m.s.d. from idealized geometry	
bond (Å)	0.0031 ± 0.0002
bond angles (°)	0.366 ± 0.04
improper torsions (°)	0.171 ± 0.03
R.m.s.d. from experimental constraints[b]	
distances (Å)	0.030 ± 0.002
Final energies	
E_{total}	206 ± 8
E_{bonds}	15 ± 3
E_{angles}	73 ± 4
$E_{impropers}$	4 ± 1
E_{vdW}	55 ± 3
E_{NOE}	59 ± 9
Coordinate precision[c] (Å)	
r.m.s.d. of backbone atoms (N, Cα, C′) excluding all residues not part of secondary structure	0.55 Å ± 0.11
r.m.s.d. of all heavy atoms excluding all residues not part of secondary structure	1.38 Å ± 0.18

[a]<SA> represents the ensemble of the 20 final structures. Force constants used to calculate energy terms are the same as published previously (Holak *et al*., 1989; Stoll *et al*., 1997).
[b]No distance restraint in any of the structure included in the ensemble was violated by >0.5 Å. The r.m.s.d. of the interproton distance restraints was calculated as described (Holak *et al*., 1989).
[c]R.m.s.d. between the ensemble of structures <SA> and the average structure of the ensemble $<SA>_{av}$.

Dynamic properties

^{15}N-T_2, ^{15}N{^{1}H}-NOE and ^{15}N(dipole-CSA) cross-correlation rates were determined at 600 MHz proton frequency (see Materials and methods). The steady state heteronuclear ^{15}N{^{1}H}-NOE for the backbone amides of human MIA proves that most of the 108 residues of human MIA are part of a compact fold, with the exception of residues Met1–Leu7, because relaxation data could not be extracted (residues Met1, Gly2, Met4 and Leu7) (Figure 3) nor could long range NOEs be identified. The C-terminus, apart from Gln108, does not exhibit any pronounced flexibility. This is in contrast to residues Tyr69–Ala75, which have ^{15}N{^{1}H}-NOE values <0.6. This clearly suggests an increased flexibility for this region of human MIA in agreement with the elevated ^{15}N-T_2 values for residues Asp68–Ala75 (data not shown). The ^{15}N(dipole-CSA) cross-correlation rates η not only confirm the existence of fast motions on the ps to ns time scales for this region but also indicate that small amounts of exchange broadening are present for these residues (data not shown). Apart from variations in the ^{15}N chemical shift anisotropy, which are usually small in proteins, $\eta \times T^2$ values are only influenced by slow chemical exchange (Renner and Holak, 2000). In our case, markedly decreased $\eta \times T^2$ values are observed exactly for residues D68–A75, consistent with slow motions in this region.

Bioassay and phage display

The recombinant human MIA used for structure determination was tested for biological activity with Boyden Chamber assays (Bosserhoff *et al*., 1998, 1999). The invasive potential of the melanoma cell line Mel Im was inhibited by the recombinant human MIA (rhMIA), 45.6% ± 3.1, demonstrating that the recombinant protein is as active as native MIA. Results of the phage display screening revealed a high percentage of clones carrying heptapeptides with multiple prolines. Out of 40 isolated and sequenced clones, 11 (27.5%) contained two or more prolines. Using a

Table II. Peptides tested in this study as putative ligands for human MIA

Peptides obtained from phage display		Other peptides tested in this study	Fibronectin-derived peptides tested in this study
Heptapeptides	Dodecapeptides		
VPHIPPN	QLNVNHQARADQ	RKLPPRPRR (PI3-kinase SH3 domain-binding peptide)	ETTIVITWTPAPR (FN6)
MPPTQVS	TSASTRPELHYP	VLASQIATTPSP	TSLLISWDAPAVT (FN10)
QMHPWPP	TFLPHQMHPWPP	TPLTKLPSVNHP	NSLLVSWQPPRAR (FN14)
QPPFWQF	VPHIPPNSMALT	PPNSFSSAGGQRT (control peptide 1)	
TPPQGLA	RLTLLVLIMPAP (pdp12)	EQDSRQGQELTKKGL (control peptide 2)	
IPPYNTL			
AVRPAPL			
GAKPHPQ			
QQLSPLP			
GPPPSPV			
LPLTPLP			

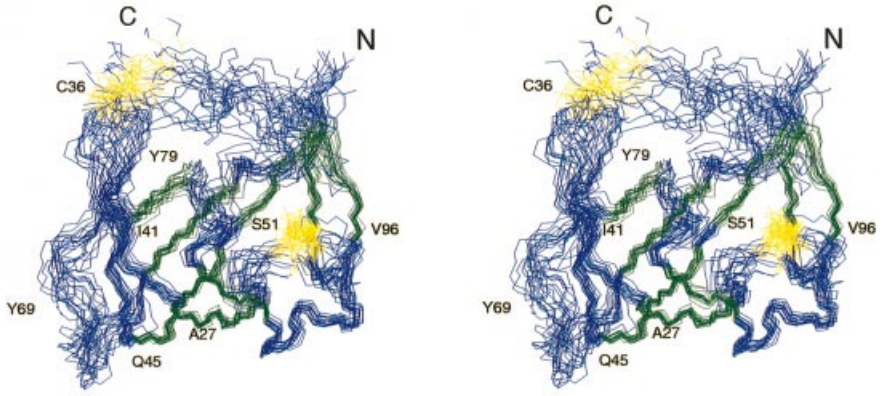

Fig. 1. Stereoview of the backbone atoms (N, C^{α}, C′, O) of all residues for the ensemble <SA> of 20 structures of human MIA best fitted to N, C^{α} and C′ atoms of the regions with regular secondary structure (β-sheets). β-sheets are shown in green and cysteines are shown in yellow. The unstructured residues Met1–Leu7 are omitted for clarity. The N- and C-termini of human MIA are indicated by N and C, respectively. This figure was generated with MOLMOL (Koradi *et al*., 1996).

dodecapeptide phage display library, five sequences have been identified including the peptide pdp12 (RTLLVLIMPAP) (Table II; Figure 5). An 'empty phage' was used as a negative control. All peptides tested in this study are given in Table II.

Fluorescence spectroscopy

In contrast to the heptapeptides, peptide pdp12 obtained from the dodecapeptide phage display library is insoluble in aqueous solution at the concentration required for multi-dimensional NMR spectroscopy, even in the presence of 40% dimethylsulfoxide (DMSO). This prevented ligand binding studies by NMR. Therefore, the interaction of the peptide pdp12 and human MIA was investigated by fluorescence spectroscopy. The blue shift of the protein tyrosine and tryptophan fluorescence is 4 nm and of the protein tryptophan fluorescence is 6 nm upon titration with the peptide pdp12. The dodecapeptides VLASQIATTPSP and TPLTKLPSVNHP were used as control peptides and did not show any affinity for human MIA. Similarly, the dodecapeptides obtained from the phage display experiment, other than pdp12, showed no affinity (data not shown).

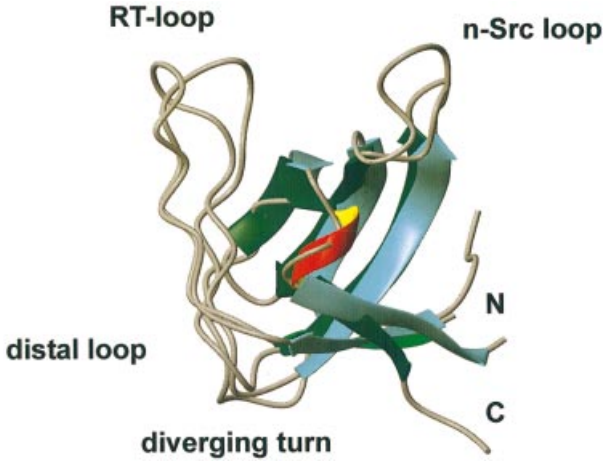

Fig. 2. Ribbon drawing of the energy-minimized mean core solution structure $(SA)_m$ of human MIA (light green) superimposed with the SH3 domain of the ABL tyrosine kinase (dark green) using the coordinates 1ABO (Musacchio *et al*., 1994). The N- and C-termini are indicated by N and C, respectively. Secondary structural elements are colored in red (helices) and green (β-strands). This figure was generated with MOLMOL (Koradi *et al*., 1996).

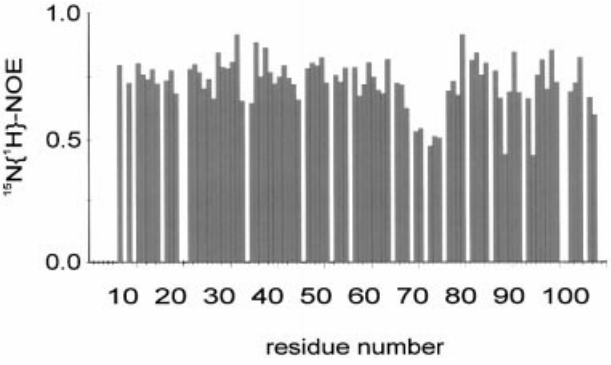

Fig. 3. Steady state heteronuclear ^{15}N{^{1}H}-NOE for the backbone amides of human MIA. Residues for which no results are shown correspond either to prolines or to residues where relaxation data could not be extracted.

ELISA assay for protein–protein interaction

A quantitative immunoassay was designed to investigate the interaction between MIA and fibronectin. Different ECM molecules were coated onto a plastic surface and exposed to MIA. The amount of MIA that was bound to the coated ECM molecule was measured by a peroxidase-linked monoclonal MIA antibody. Results shown in Table III reveal that MIA binds specifically to surfaces coated with fibronectin, but not to collagen type I, heparansulfate proteoglycane (HSPG) or bovine serum albumin (BSA). To prove further that the binding is specific and not due to a sticky effect of ECM proteins, the binding assays were performed with denatured MIA protein. Denatured MIA protein is still detected by the polyclonal antibody used in the assay, but the 3D structure is destroyed. Denatured MIA was not able to bind to any of the matrix proteins tested (data not shown).

Table III. Interaction between MIA and ECM molecules

Matrix protein	Control	Plus MIA	Fold difference
Fibronectin	0.115 ± 0.013	2.086 ± 0.063	18.1
Collagen type I	0.113 ± 0.021	0.145 ± 0.032	1.3
HSPG	0.098 ± 0.012	0.104 ± 0.016	1.1
BSA	0.113 ± 0.017	0.114 ± 0.022	1.0
MIA	2.423 ± 0.069	2.523 ± 0.075	1.0

Matrix proteins coated onto 96-well plates were exposed to 50 ng/ml purified MIA (plus MIA). MIA binding was quantified using a peroxidase-coupled monoclonal anti-MIA antibody and the substrate ABTS (Roche). Control reactions show binding of the antibody to the respective matrix proteins exposed to 50 ng/ml BSA instead of MIA. Values indicate OD at 405 nm.

Discussion

The core structure of human MIA in solution resembles a Src homology 3 (SH3) domain as shown by a DALI database search (Holm and Sander, 1993) (Figures 1 and 2). The r.m.s.d. of both structures superimposed is 1.4 Å. Based on the 3D structure, the amino acid sequence of human MIA can be aligned with other amino acid sequences known to adopt the same fold, such as the SH3 domains of the ABL and FYN tyrosine kinases (Figure 4). SH3 domains are small (55–70 amino acids) non-catalytic protein modules that are found in many intracellular signaling proteins (Koch *et al*., 1991; Yu *et al*., 1992, 1994). SH3 domains mediate protein–protein interactions by binding to Pro-rich peptide sequences (Dalgarno *et al*., 1997). More than fifty SH3 domains are known and these SH3 domains are widely distributed, having been identified in kinases, lipases, GTPases, adapter proteins, structural proteins and viral regulatory proteins (see, for example, Musacchio *et al*., 1994; Dalgarno *et al*., 1997). To our knowledge, no extracellular SH3 domain has been described so far. Therefore, human MIA appears to be the first extracellular protein adopting an SH3 domain-like fold in solution.

Human MIA shares the common fold of SH3 domains, consisting of two perpendicular, antiparallel, three-stranded β-sheets. Based on the first description of the SH3 structure, the strands of the β-sandwich in the core of human MIA are termed βa, βb, βb′, βc, βd, βe and β_{irr} (Yu *et al*., 1992; Dalgarno *et al*., 1997). These β-strands form two β-sheets, βI and βII. The smaller βI is formed by a part from βb, βa and βe. The strand βII contains the remainder of βb′, βc and βd, as well as βnt/βct. The portions of the βb/b′-strand participating in both βI and βII are delineated by a kink, which changes the direction of the polypeptide. The β-strands pack against each other at approximately right angles to form a β-sandwich.

Two characteristic features of SH3 domains, the RT-loop and the n-Src loop, can be identified in human MIA (Figures 1, 2 and 4) (Yu *et al*., 1992; Dalgarno *et al*., 1997). The RT-loop contains an irregular antiparallel structure. In human MIA, a short antiparallel β-sheet β_{irr} could be detected for Asp30–Met32 and Thr40–His42, found in only a few SH3 domains (Martínez and Serrano *et al*., 1999; Riddle *et al*., 1999). βc and βd form the distal hairpin, the most regular element of secondary structure in the SH3 domain (Riddle *et al*., 1999). βc and βd are connected by a tight type I β-turn in the SH3 domain (Musacchio *et al*., 1994; Martínez *et al*., 1999; Riddle *et al*., 1999). In human MIA, this distal loop comprises the residues Tyr69–Ala75, which exhibit an increased flexibility. The steady state heteronuclear ^{15}N{^{1}H}-NOE values for residues Tyr69–Ala75 are <0.6, clearly indicating a higher degree of flexibility (Figure 3). The ^{15}N relaxation data showing flexibility in the distal loop region are useful in assessing the structure, given the lack of precision of structure determination in the distal region (Figure 3). In human MIA, an additional antiparallel β-sheet βnt/βct is present, which is located at the N- and C-terminus and belongs to strand βII (Figures 1 and 2). This β-sheet is not found in other SH3 domains. All β-sheet residues identified for human MIA are well conserved in different species such as mouse, rat and cow (Figure 4). Another interesting feature of human MIA is its disulfide bonding pattern, Cys13–Cys18 and Cys36–Cys107. In SH3 domains, disulfide bridges have not been described so far. In human MIA, they account for the fact that this SH3 domain with an additional β-sheet occurs in the extracellular space physiologically (Bosserhoff *et al*., 1997, 1998, 1999). Residues Met1–Leu7 do not adopt any regular structure in structure calculations, either due to missing assignments or to

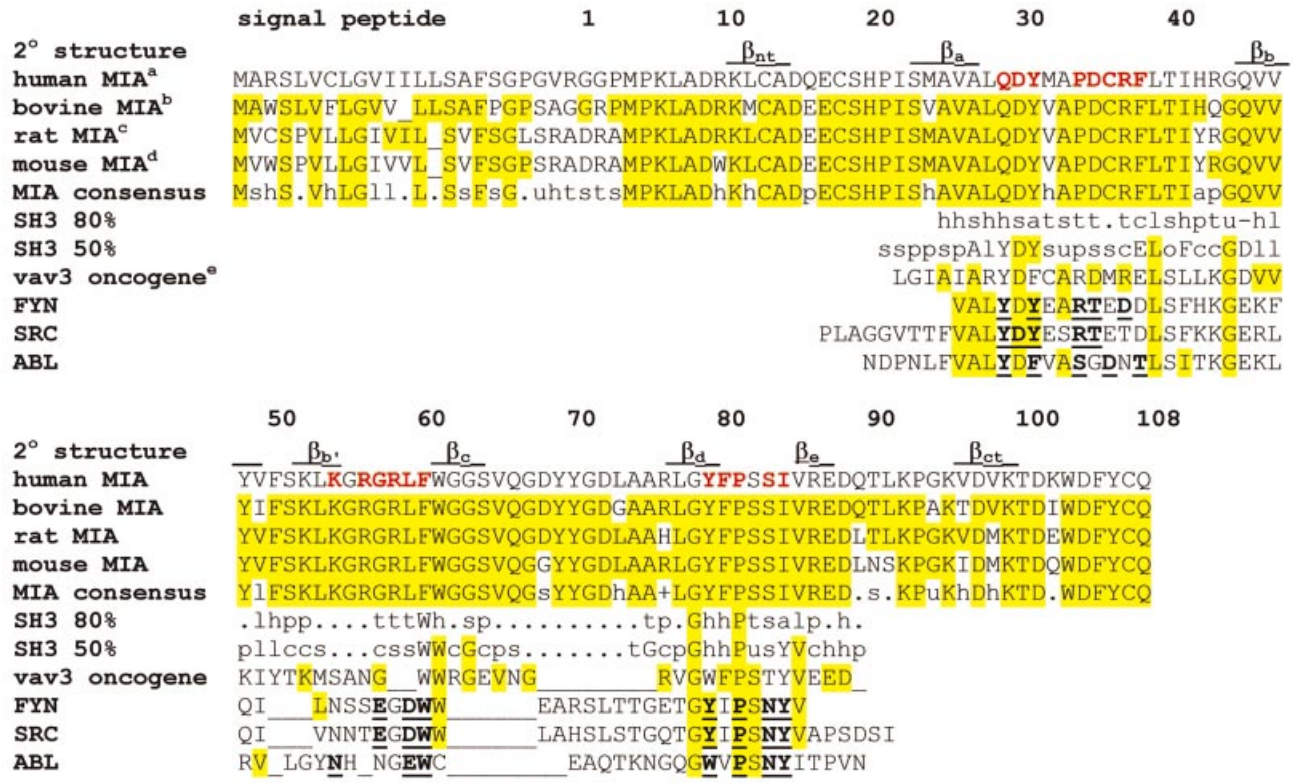

Fig. 4. Sequence alignment of MIA and representative SH3 sequences. Bold underlined residues of FYN, SRC and ABL mark peptide substrate-binding residues. Red characters of the human MIA sequences mark residues that match peptide substrate-binding residues of other SH3 domains. Residues in the alignment highlighted in yellow are identical to the human MIA sequence. To compare the MIA sequences with known SH3 sequences, consensus sequences for the five MIA sequences and 289 SH3 domain sequences were obtained from the Web-based server SMART (Schultz *et al*., 2000). The human MIA sequence generated a prediction of an SH3 fold by the 3D-PSSM Web server (Kelley *et al*., 2000), with the best-scoring hit obtained from the vav-3 oncogene sequence. The ABL, FYN and SRC sequences represent hits from the structure similarity search program DALI (Holm and Sander, 1993). The similarities between the MIA and SH3 sequences, especially at the first and third substrate binding regions (the 'RT-loop' and βd regions, respectively) demonstrate the SH3 conformity and support the prediction of MIA substrate binding residues. The second substrate binding region (the 'n-Src loop'), often with a characteristic Trp–Trp pair, is more variable among SH3 sequences and is also more distinct for the MIA sequences. Variable insertions at this segment prevent a unique alignment of all sequences. An overlay of the 3D structures places two MIA phenylalanine residues in positions with a potential to interact with substrates. One of these phenylalanine residues corresponds to the SH3 substrate-binding tryptophan of the n-Src loop, and the other in the third substrate binding region as also found in the vav-3 oncogene sequence ([a,d]Bosserhoff *et al*., 1997; [b]Dietz *et al*., 1996; [c]J.X.Lu, unpublished; [e]Movilla and Bustel, 1999). Consensus code: o, alcohol; l, aliphatic; a, aromatic; c, charged; h, hydrophobic; –, negative; p, polar; +, positive; s, small; u, tiny; t, turn-like.

absent NOEs in the NOESY spectra, and were therefore omitted for clarity in Figure 1.

Unlike all SH3 domains known so far, human MIA is a single-domain globular protein of 12 kDa that adopts an SH3 domain-like fold in solution. Therefore, this is the first description of an SH3 domain with an additional β-sheet that is not a module of a larger protein (Dalgarno *et al*., 1997). Furthermore, based on the tertiary and secondary structure, the amino acid sequence of human MIA can be aligned to other SH3 domains, for example, ABL and FYN (Figure 4). A schematic representation of the energy-minimized mean solution structure $(SA)_m$ of human MIA in comparison with the c-Src SH3-domain fold is shown in Figure 2 (Yu *et al*., 1992; Musacchio *et al*., 1994). The ligand binding site of SH3 domains is a relatively flat surface, and one end is flanked by the RT-loop and the n-Src insertion, both of variable length (Musacchio *et al*., 1994; Dalgarno *et al*., 1997) (Figures 4 and 5). Most of the residues of the binding site of SH3 domains are conserved in the sequence of human MIA (Figures 4 and 6) (Musacchio *et al*., 1994; Dalgarno *et al*., 1997; Mongiovi *et al*., 1999). In addition, all residues of human MIA that can be aligned to residues of ABL and FYN known to bind to Pro-rich peptides are close in space and form a putative binding site on human MIA (Figures 4 and 6). The peptides identified as ligands for human MIA in the heptapeptide phage display experiment are strikingly similar to the consensus sequence XPPLPXR for SH3 domains, especially for the motif XPpXP and otherwise mostly hydrophobic residues such as Val, Thr and Leu (Feng *et al*., 1994; Musacchio *et al*., 1994; Yu *et al*., 1994; Dalgarno *et al*., 1997; Mongiovi *et al*., 1999) (Table II; Figure 5). However, none of the heptapeptides led to chemical shift perturbations in a ^{1}H-^{15}N HSQC when titrated to a uniformly ^{15}N-enriched sample of human MIA, even in a 10- to 20-fold molar excess. This difference in binding between the phage peptides and the free peptides is likely to be due to avidity effects resulting from polyvalent display on phage. Obviously, the affinity of the heptapeptides is not sufficient, albeit there is a resemblance of these peptides to the consensus sequence for SH3 domains. Figure 6 shows the contact surface of human MIA (A) in comparison with that of 1ABO (B) (Musacchio *et al*., 1994). In contrast to the ABL domain,

the human MIA protein does not share the feature of an acidic patch around the n-Src loop. In fact, the n-Src loop of human MIA is characterized by a predominantly basic patch. This might explain why the commercially obtained PI3-kinase SH3 domain-binding peptide, RKLPPRPRR, did not produce NMR chemical shift perturbations in MIA.

The peptide pdp12 obtained from the dodecapeptide library was further analyzed by fluorescence spectroscopy. The fluorescence maximum of human MIA at 345 nm indicates that the tryptophans are partially solvent exposed, in agreement with the NMR solution structure. The titration of human MIA with the peptide pdp12 leads to a shift of the observed fluorescence maximum from 345 to 339 nm. This blue shift indicates that the tryptophans are shielded from solvent upon binding of the peptide to human MIA (Lakowicz, 1983). The fluorescence data suggest a model where MIA binds the peptide pdb12 in the consensus binding site of SH3 domains, as the conserved Trp61 is located in its center. However, the other tryptophan in MIA, Trp103, which is located distant from Trp61, may indicate that additional residues of human MIA are involved in binding to its ligand.

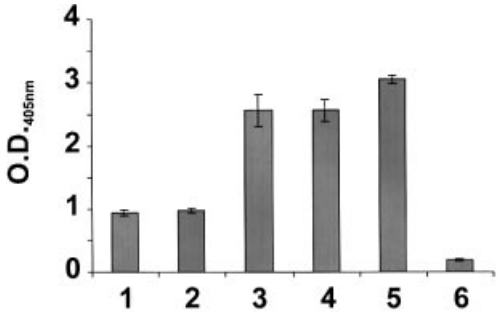

Fig. 5. Phage display screening results using a dodecapeptide phage display library. 1, QLNVNHQARADQ; 2, TSASTRPELHYP; 3, TFLPHQMHPWPP; 4, VPHIPPNSMALT; 5, RLTLLVLIMPAP (pdp12); 6, 'empty phage' as negative control. For details see text.

A sequence database search revealed a high similarity of the peptide pdp12 to the B strand of human fibronectin (FN) type III repeats (Figure 7). In addition, the ELISA data clearly show that human MIA binds to fibronectin, but not to collagen type I or HSPG (Table III). BSA and MIA were used as negative and positive controls. Hence, we provide evidence that the MIA protein specifically binds to fibronectin in the ECM. As denatured MIA did not bind to any of the matrix proteins tested (data not shown), the specific binding of MIA to fibronectin was supported further. In order to map the binding site of human MIA on fibronectin, we synthesized three peptides derived from the fibronectin sequence (Table II). These peptides comprised the sequences of fibronectin best matching the pdp12 peptide found in FN type III repeats 6, 10 and 14 (Figure 7). In order to test the functionality of the fibronectin-derived sequence, the ELISA was performed in the presence of the competitive peptide (Figure 8). The fibronectin-derived peptides FN6, FN10 and FN14 interfere competitively with binding of MIA to fibronectin in

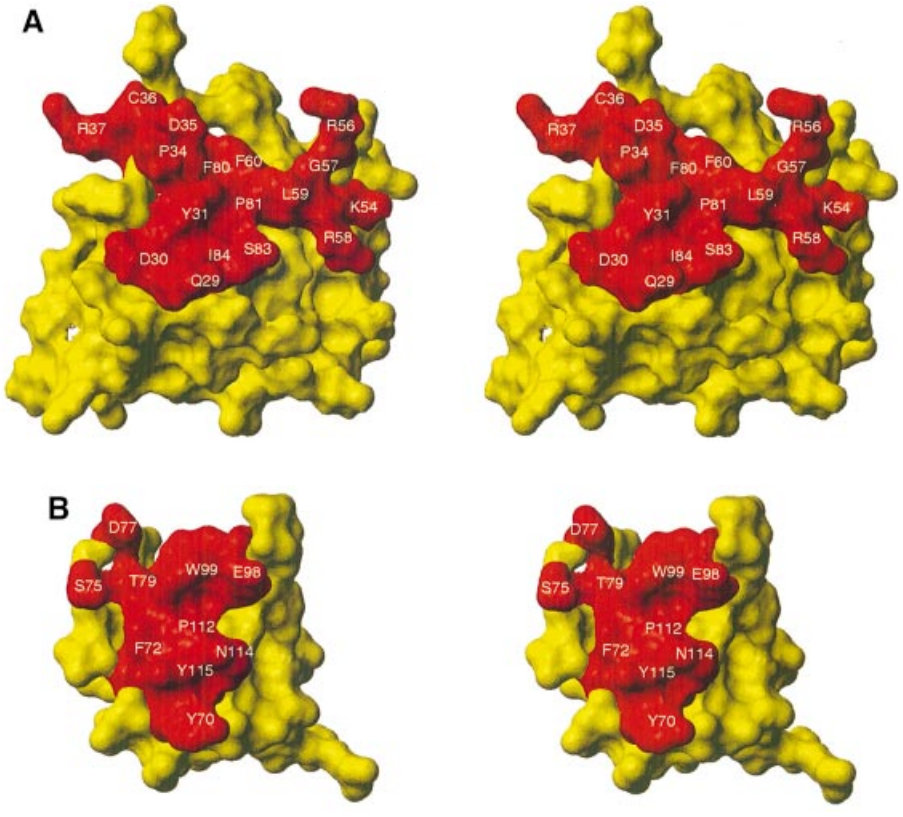

Fig. 6. Stereo contact surfaces of human MIA (residues 8–108) (**A**) and 1ABO (**B**) generated with MOLMOL (Koradi *et al*., 1996). The atom radius was set to the van der Waals value and the solvent radius to 1.4 Å. Residues that determine specificity of SH3 domains for their target peptides are shown in red. For human MIA, residues that match peptide substrate binding residues of other SH3 domains are also colored in red. The view is almost identical to Figures 1 and 2. For details see text and Figure 4.

```
FN1         SQPNSHPIQWNAPPQSH
FN2         AS..SFVVSWVSA.SDT
FN3         DT..SIVVRWSRP.QAP
FN4         DV..KVTIMWTPP.ESA
FN5         DS..TVLVRWTPP.RAQ
FN6         TET.TIVITWTP...AP
FN7         DTG.VLTVSWERSTTPD
FNEBD       DS..SIGLRWTPLNSST
FN8         PD..TMRVTWAPPPSID
FN9         AN..SFTVHWIAP.RAT
FN10        PT..SLLISWDAP.AVT
FN11        DN..SISVKWLPS.SSP
FNEDA       VD..SIKIAWESP.QGQ
FN12        PT..SLSAQWTPP.NVQ
FN13        ET..TITISWRTK.TET
FN14        PN..SLLVSWQPP.RAR
FN15        ALS.QTTISWAP..FQD

consensus   ....ohxhohxPP....

pdp12       ..RLTLLVLIMPAP...
```

Fig. 7. A structure-based sequence alignment of parts of 17 type III human FN repeats taken from the Swiss-Prot accession No. P02751. Residues in green are part of a β-strand. Residues in red are implicated in integrin binding. The symbols of the consensus sequence indicate *h* for hydrophobic, o for Ser or Thr, and P for Pro (Sharma *et al*., 1999). The sequence of the target peptide pdp12 of human MIA is aligned according to the consensus sequence.

the ELISA in a dose-dependent manner, suggesting that the peptide binds to MIA and blocks the binding site for the fibronectin target sequence (Figure 8). This provides evidence for binding of MIA to the B strand of human fibronectin type III repeats of, at least, FN6, FN10 and FN14.

A 30 kDa heparin-binding fragment of FN containing FN12–14 has been isolated and shown to support heparin-dependent adhesion of melanoma and neuroblastoma cells (Benecky *et al*., 1988; McCarthy *et al*., 1988; Ingham *et al*., 1990; Barkalow *et al*., 1991; Drake *et al*., 1993). In addition to the known heparin-binding capability of FN12–14, several reports have indicated that it may possess binding sites for integrins (Mould and Humphries, 1991; Mohri *et al*., 1996a,b). Cell adhesion to this segment involves the synergistic interaction of the cell surface integrin $\alpha_4\beta_1$ and heparan sulfate proteoglycans (Mould *et al*., 1994). Functional data suggest that FN12–14 is able to promote melanoma cell adhesion activity and is sensitive to anti-α_4 and anti-β_1 antibodies, suggestive of a direct interaction between FN12–14 and $\alpha_4\beta_1$ (Mould and Humphries, 1991). Based on alanine mutations, it was recently shown that in FN14 the sequence PRARI, connected to Asp184 by hydrogen bonds, plays a similar role in binding to integrins to the synergy sequence PHSRN in FN9 (Sharma *et al*., 1999). Whereas PHSRN is known to interact directly with the integrins $\alpha_5\beta_1$ and $\alpha_{IIb}\beta_3$, the sequence PRARI was shown to interact with integrin $\alpha_4\beta_1$ (Sharma *et al*., 1999). This RAR sequence is in proximity to the target peptide of human MIA located in FN14. Therefore, while bound to FN14, human MIA might interfere sterically with the binding of FN to integrin $\alpha_4\beta_1$.

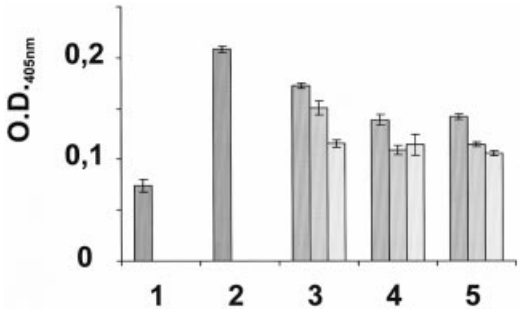

Fig. 8. Test of functionality of fibronectin-derived peptides. 1, BSA; 2, MIA; 3, FN14; 4, FN10; and 5, FN6. For the fibronectin-derived sequences a titration was performed by adding 1, 2 and 4 µl of the peptide stock solution to the assay (from left to right in 3, 4 and 5). For details see text.

Intact FN has binding surfaces for several molecules, including collagens, fibrin, integrins, heparin, DNA, etc. *In vivo*, it may be occupied at multiple sites by multiple ligands. This might also be true for binding of human MIA to FN, as the identified target peptides share sequence similarities with all FN regions shown in Figure 6. The matching sequence of all human type III FN repeats suggests the intriguing possibility of multiple binding of human MIA to several FN repeats, but at least to FN6, FN10 and FN14, inhibiting the binding of integrins to FN and thereby detaching cells from the ECM (Potts and Campbell, 1994; Grant *et al*., 1997; Bosserhoff *et al*., 1999).

In conclusion, our study provides evidence for the molecular mechanism of MIA in promoting invasion and metastasis *in vivo* by binding to human fibronectin type III repeats, thereby inhibiting attachment of melanoma cells. Therefore, the structure of human MIA may suggest a new mechanism of metastasis: binding of this extracellular SH3-like domain to type III repeats of fibronectin competes with integrin binding, thus detaching cells from the ECM (Potts and Campbell, 1994; Grant *et al*., 1997; Bosserhoff *et al*., 1999).

Materials and methods

Cloning of human MIA

The recombinant human MIA protein was obtained from an *Escherichia coli* BL21(pUBS 520) expression system and comprised the human MIA open reading frame from amino acid G25 to Q131 plus an additional N-terminal methionine cloned in a modified pQE-40 vector (Qiagen), resulting in a primary structure of Met1 to Gln108 of the polypeptide used in this study (Brinkmann *et al*., 1989). The construct was checked by dideoxy DNA sequencing and was shown not to carry any mutation (data not shown).

Expression, refolding and purification of human MIA

Expression, refolding and purification of human MIA was performed as previously described (Mühlhahn *et al*., 1998; Stoll *et al*., 2000). Typically, NMR samples contained 1 mM protein in 100 mM potassium phosphate and 150 mM NaCl pH 7.0, including 0.02% NaN_3 and protease inhibitors (Roche Molecular Biochemicals). Purified protein was checked by SDS–PAGE, MALDI-TOF and N-terminal amino acid sequencing according to Edman and was shown to be 95% pure (data not shown). All protein samples used for NMR spectroscopy contained 10 or 100% D_2O.

NMR spectroscopy

NMR experiments were carried out at 300 K on Bruker AMX 500, DRX 500, DRX 600 and DMX 750 spectrometers. For backbone assignment, triple resonance experiments CBCA(CO)NH, CT-HNCA and CT-HNCO

were recorded (Grzesiek and Bax, 1992a,b). Water suppression in experiments recorded on samples in H_2O was achieved by incorporation of a Watergate sequence into the various pulse sequences (Braunschweiler and Ernst, 1983; Bax and Davis, 1985; Shaka *et al*., 1988; Sklenar *et al*., 1993). Triple resonance experiments, 2D total correlation spectroscopy (TOCSY) (τ_m = 53 ms), 3D ^{1}H-^{15}N TOCSY-HSQC (τ_m = 50 ms), long mixing time 2D NOESY (τ_m = 120 ms) and long mixing time 3D ^{1}H-^{15}N NOESY-HSQC (τ_m = 120 ms) experiments in H_2O were recorded in a water flip-back version (Braunschweiler and Ernst, 1983; Bax and Davis, 1985; Shaka *et al*., 1988; Marion *et al*., 1989a,b; Sklenar *et al*., 1993; Jahnke *et al*., 1995; Lippens *et al*., 1995; Dhalluin *et al*., 1996; Talluri and Wagner, 1996). Side chain resonances were assigned using 2D NOESY (τ_m = 120 ms) in D_2O, 3D ^{1}H-^{15}N TOCSY-HSQC and 3D ^{1}H-^{15}N NOESY-HSQC experiments. Stereospecific assignments were obtained from a combination of 2D double quantum filter-correlated spectroscopy (DQF-COSY) and short mixing time 2D NOESY in D_2O, short mixing time 3D ^{1}H-^{15}N NOESY-HSQC (τ_m = 50 ms) in H_2O, 2D $^1H^N$-^{15}N-[$^{13}C^\gamma$] difference HSQC and 2D $^{13}C'$-[$^{13}C^{\gamma[aromatics]}$] spin-echo difference together with 2D ^{15}N-[$^{13}C^{\gamma[aromatics]}$] spin-echo difference $^1H^N$-^{15}N HSQC experiments (Rance *et al*., 1983; Hu and Bax, 1997; Hu *et al*., 1997). 2D ^{1}H-^{15}N HSQC spectra with reduced signal loss due to the fast chemical exchange were recorded using procedures described previously (Mori *et al*., 1995). All 3D spectra were processed and evaluated with the software CC-NMR (Cieslar *et al*., 1993). Exchange rates of ^{1}H-^{15}N-bound protons were measured by recording a series of 2D ^{1}H-^{15}N HSQC spectra at 15 min, 28 h, 1 day, 1 week and 1 month after dissolving the protein in D_2O. For example, in the exchange experiment the following 35 amide resonances were still visible in a ^{1}H-^{15}N HSQC 28 h after dissolving a lyophilized protein sample in D_2O at 300 K, pH 7.0: Lys11, Leu12, Cys13, Ile22, Ser23, Ala25, Val26, Ala27, Gln29, Tyr31, Phe38, Ile41, Gln45, Leu39, Val47, Tyr48, Val49, Phe50, Ser51, Lys52, Leu53, Lys54, Trp61, Gly62, Gly63, Ser64, Asp68, Tyr70, Tyr79, Phe80, Ile84, Val85, Arg86, Asp88 and Val98. Modified versions of the experiments proposed previously were used to determine ^{15}N-T_2, ^{15}N{^{1}H}-NOE and ^{15}N(dipole-CSA) cross-correlation rates at 600 MHz proton frequency (Edison *et al*., 1994; Farrow *et al*., 1994; Tessari *et al*., 1997; Renner and Holak, 2000). Relaxation periods of 16 ms + x $\times$ 32 ms for T_2, with x = 0, 1, 2, 3, 4, were used (Jones *et al*., 1996). The relaxation delays used for the cross-correlation experiments were 40 and 80 ms. Most relaxation experiments were recorded in an interleaved manner to reduce influence from possible instabilities in experimental conditions. NOE values were calculated from the ratio of the peak heights in the experiment with and without proton saturation. To obtain T_2 values, the experimental data points (peak heights) were fitted to a curve $A \exp(-t/T_2)$ with a simple grid search. Uncertainties were determined from double recording either of single data points or the whole relaxation experiment. For the cross-correlation rates η, the ratios of signal intensities (peak heights) from the cross-correlation experiment and the corresponding reference experiment follow a simple linear relation, $T \times \eta$ (Tessari *et al*., 1997). The difference between the rates η obtained from the experiments with different relaxation delays served as an error estimate.

Assignment and structure calculation

Assignment, data handling and control of X-PLOR calculations were performed using our software NMRXplorer, which is based on CC-NMR (Brünger, 1993; Cieslar *et al*., 1993). NOEs were derived from the 2D NOESY spectra in H_2O and D_2O, and from the ^{15}N-edited and the ^{13}C-edited NOESY spectra. Peak heights were used for quantification of peak intensities. Five classes of NOEs were distinguished, as previously described (Stoll *et al*., 1997). Sequential $H^\alpha(i)$-$H^N(i+1)$ signals within β-elements were rated as strong NOEs; other NOE intensities were then ascribed according to this internal calibration. The upper and lower (in parentheses) tolerances for these distance restraints were set to 1.8 Å (0.6), 0.5 Å (0.5), 0.4 Å (0.4), 0.3 Å (0.3) and 0.3 Å (0.3), respectively. All protons were explicitly defined in the dynamically simulated annealing calculations; in some cases, however, additional terms were added to the upper bounds as a pseudoatom correction (Wüthrich, 1986).

The distance constraints were supplemented with 22 θ torsion angle constraints derived from the HNHA experiment (Vuister and Bax, 1993). Structure calculations were performed using standard protocols for simulated annealing constraint methods implemented in the program X-PLOR (Holak *et al*., 1989).

Ligand binding

NMR titrations using putative peptide ligands consisted of monitoring changes in chemical shifts and line widths of the backbone amide resonances of uniformly ^{15}N-enriched MIA samples, in a series of HSQC spectra, as a function of ligand concentration following the procedure of 'SAR by NMR' (McAlister *et al*., 1996; Shuker *et al*., 1996). Quantitative analysis of ligand-induced shifts was performed by applying the equation of Pythagoras to weighted chemical shifts: $\Delta\delta_c(^1H, ^{15}N) = [\{|\Delta\delta(^1H)|^2 + 0.2 \times |\Delta\delta(^{15}N)|^2\}^{0.5}]$. Only $\Delta\delta_c(^1H, ^{15}N)$ values >0.1 p.p.m. were considered to be significant. All peptides tested for binding to human MIA were synthesized on solid phase and purified by reversed phase chromatography.

Bioassay

To test recombinant human MIA used for structure determination, Boyden Chamber assays were performed to prove its biological activity (Bosserhoff *et al*., 1998). Briefly, invasion assays were performed in Boyden Chambers containing polycarbonate filters with 8 µm pore size (Costar, Bodenheim, Germany) essentially as described previously (Albini *et al*., 1987; Jacob *et al*., 1995). Filters were coated with a commercially available reconstituted basement membrane (Matrigel, diluted 1:3 in H_2O; Becton Dickinson, Heidelberg, Germany). The lower compartment was filled with fibroblast-conditioned medium as a chemoattractant. Melanoma cells were harvested by trypsinization for 2 min, resuspended in Dulbecco's modified Eagle's medium (DMEM) without fetal calf serum (FCS) at a density of 2×10^5 cells/ml, with or without recombinant human MIA (50 ng/ml), and placed in the upper compartment of the chamber. After incubation at 37°C for 4 h, filters were removed. Cells adhering to the lower surface were fixed, stained and counted.

Phage display

Phage display screening was performed using heptapeptide and dodecapeptide phage display libraries (BioLabs, Beverly, CA) following the manufacturer's instructions. Recombinant human MIA was coated onto the wells of a high protein-binding 96-well plate at a concentration of 10 µg per well. Binding phages were selected by incubation in the MIA-coated plates for 60 min at room temperature. For each selection, 2×10^{11} phages were added per well. Non-binding phages were removed by washing five times with TBS for 10 min; bound phages were eluted by adding rhMIA at a concentration of 100 µg/ml. The eluted phages were amplified and the biopanning was repeated four times. The binding clones were characterized by sequencing the phage insert.

Fluorescence spectroscopy

Fluorescence data were collected on a Perkin Elmer luminescence spectrometer LS50B at 300 K, with emission and excitation bandpasses set to 2.5 nm. Emission was set to 280 or 295 nm to minimize interference from the protein tyrosine fluorescence, and emission spectra were recorded from 300 to 400 nm. All samples contained 10 mM Tris–HCl pH 7.0 and the peptide ligand of interest including 1% DMSO. Human MIA protein and the peptide ligands (in 100% DMSO) were diluted from stock solution to give a final concentration of 3 µM and up to 50 µM, respectively. All final spectra were difference spectra corrected for the native peptide fluorescence, buffer and DMSO effects. Under these conditions, the fluorescence observed can be attributed to the fluorophores of the human MIA protein.

Assays for protein–protein interaction

Protein–protein interaction assays were performed in 96-well plates. Wells were coated with fibronectin (1 µg/cm^2), collagen type I (1 µg/cm^2) or HSPG (2 g/cm^2) by incubation at 4°C for 12 h. Non-specific binding of cells was blocked by pre-incubation of the wells with 3% BSA/phosphate-buffered saline (PBS) for 2 h. The matrix proteins were exposed to 50 ng/ml purified MIA for 30 min. MIA binding was quantified using a peroxidase-coupled monoclonal anti-MIA antibody and the substrate ABTS (Roche). Controls were exposed to 50 ng/ml BSA or to denatured MIA instead of native MIA. Reactions were quantified at an OD of 405 nm. Functionality of the peptides was tested in the protein–protein interaction assay by the addition of aliquots of a 1 µg/ml peptide stock solution. Two control peptides derived from the transmembraneous receptor protein ILA (control peptide 1, PPNSFSSAGGQRT; control peptide 2, EQDSRQGQELTKKGL) were used as negative controls.

Coordinates

The coordinates of <SA> and $(SA)_m$ of human MIA have been deposited in the Protein Data Bank under accession number 1HJD.

Acknowledgements

R.S. gratefully recognizes support from the Studienstiftung and the Fonds der Chemischen Industrie. This work was supported by DFG grants (SFB 469 and BO 1573/1-1) and the Deutsche Krebshilfe (10-1532-Bo).

References

Albini,A. Iwamoto,Y., Kleinman,H.K., Martin,G.R., Aaronson,S.A., Kozlowski,J.M. and McEwan, R.N. (1987) A rapid *in vitro* assay for quantitating the invasive potential of tumour cells. *Cancer Res.*, **47**, 3239–3245.

Barkalow,F.J. and Schwarbauer,J.E. (1991) Localization of the major heparin-binding site in fibronectin. *J. Biol. Chem.*, **266**, 7812–7818.

Bax,A. and Davis,D.G. (1985) MLEV-17-based two-dimensional homonuclear magnetization transfer spectroscopy. *J. Magn. Reson.*, **65**, 355–360.

Benecky,M.J., Kolvenbach,C.G., Amrani,D.L. and Mosesson,M.W. (1988) Evidence that binding to the carboxy-terminal heparin-binding domain (HepII) dominates the interaction between plasma fibronectin and heparin. *Biochemistry*, **27**, 7565–7571.

Blesch,A. *et al.* (1994) Cloning of a novel malignant melanoma-derived growth regulatory protein, MIA. *Cancer Res.*, **54**, 5695–5701.

Bogdahn,U., Apfel,R., Hahn,M., Gerlach,M., Behl,C., Hoppe,J. and Martin,R. (1989) Autocrine tumour cell growth inhibiting activities from human malignant melanoma. *Cancer Res.*, **49**, 5358–5363.

Bosserhoff,A.K., Kaufmann,M., Kaluza,B., Bartke,I., Zirngibl,H., Hein,R., Stolz,W. and Buettner,R. (1997) Melanoma-inhibiting activity, a novel serum marker for progression of malignant melanoma. *Cancer Res.*, **57**, 3149–3153.

Bosserhoff,A.K., Golob,M., Buettner,R., Landthaler,M. and Hein,R. (1998) MIA (Melanoma Inhibitory Activity). Biological functions and clinical relevance. *Hautarzt.*, **49**, 762–769.

Bosserhoff,A.K., Golob.,M., Hein,R. and Buettner,R. (1999) Analysis of cell signalling by MIA in active detachment of melanoma cells. *J. Invest. Dermatol.*, **113**, 74.

Braunschweiler,L. and Ernst,R.R. (1983) Coherence transfer by isotropic mixing: application to proton correlation spectroscopy. *J. Magn. Reson.*, **53**, 521–528.

Brinkmann,U., Mattes,R.E. and Buckel,P. (1989) High-level expression of recombinant genes in *Escherichia coli* is dependent on the availability of the *dnaY* gene product. *Gene*, **85**, 109–114.

Brünger,A.T. (1993) *X-PLOR Version 3.1: System for X-ray Crystallography and NMR*. Yale University Press, New Haven, CT.

Cieslar,C., Ross,A., Zink,T. and Holak,T.A. (1993) Efficiency in multidimensional NMR by optimized recording of time point-phase pairs in evolution periods and their selective linear transformation. *J. Magn. Reson.*, **101**, 97–101.

Dalgarno,D.C., Botfield,M.C. and Rickles,R.J. (1997) SH3 domains and drug design: ligands, structure, and biological function. *Biopolymers*, **43**, 383–400.

Deichmann,M., Benner,A., Bock,M., Jackel,A., Uhl,K., Waldmann,V. and Naher,H. (1999) S100-β, Melanoma inhibiting activity, and lactate dehydrogenase discriminate progressive from nonprogressive American Joint Committee on Cancer stage IV melanoma. *J. Clin. Oncol.*, **17**, 1891–1896.

Dhalluin,C., Wieruszeski,J.M. and Lippens,G. (1996) An improved homonuclear TOCSY experiment with minimal water saturation. *J. Magn. Reson.*, **111**, 168–170.

Dietz,U. and Sandell,L.J. (1996) Cloning of a retinoic acid-sensitive mRNA expressed in cartilage and during chondrogenesis. *J. Biol. Chem.*, **271**, 3311–3316.

Drake,S.L., Varnum,J., Mayo,K.H., Letourneau,P.C., Furcht,L.T. and McCarthy,J.B. (1993) Structural features of fibronectin synthetic peptide FN-C/H II, responsible for cell adhesion, neurite extension and heparan binding. *J. Biol. Chem.*, **268**, 15859–15867.

Dréau,D., Bosserhoff,A.K., White,R.L., Buettner,R. and Holder,W.D. (1999) Melanoma-inhibitory activity protein, a useful marker to monitor patients treated with immunotherapy. *Oncol. Res.*, **11**, 55–61.

Edison,A.S., Abildgaard,F., Westler,W.M., Mooberry,E.S. and Markley,J.L. (1994) Practical introduction to theory and implementation of multinuclear, multidimensional nuclear magnetic resonance experiments. *Methods Enzymol.*, **239**, 3–79.

Farrow,N.A. *et al.* (1994) Backbone dynamics of a free and a phosphopeptide-complexed Src homology 2 domain studied by ^{15}N NMR relaxation. *Biochemistry*, **33**, 5984–6003.

Feng,S., Chen.,J.K., Yu,H., Simon,J.A. and Schreiber,S.L. (1994) Two binding orientations for peptides to the Src SH3 domain: development of a general model for SH3-ligand interactions. *Science*, **266**, 1241–1247.

Grant,R.P., Spitzfaden,C., Altroff,H., Campbell,I.D. and Mardon,H.J. (1997) Structural requirements for biological activity of the ninth and tenth FIII domains of human fibronectin. *J. Biol. Chem.*, **272**, 6159–6166.

Grzesiek,S. and Bax,A. (1992a) Correlating backbone amide and side-chain resonances in larger proteins by multiple relayed triple resonance NMR. *J. Am. Chem. Soc.*, **114**, 6291–6293.

Grzesiek,S. and Bax,A. (1992b) Improved 3D triple-resonance NMR techniques applied to a 31 kDa protein. *J. Magn. Reson.*, **96**, 432–440.

Holak,T.A., Gondol,D., Otlewski,J. and Wilusz,T. (1989) Determination of the complete three-dimensional structure of the trypsin inhibitor from squash seeds in aqueous solution by nuclear magnetic resonance and a combination of distance geometry and dynamical simulated annealing. *J. Mol. Biol.*, **210**, 635–648.

Holm,L. and Sander,C. (1993) Protein structure comparison by alignment of distance matrices. *J. Mol. Biol.*, **233**, 123–138.

Hu,J-.S. and Bax,A. (1997) χ^1 angle information from a simple two-dimensional NMR experiment that identifies *trans* ^3J(NC)γ couplings in isotopically enriched proteins. *J. Biomol. NMR*, **9**, 323–328.

Hu,J-.S., Grzesiek,S. and Bax,A. (1997) Two-dimensional NMR methods for determining χ^1 angles of aromatic residues in proteins from 3-bond J(C′C-γ) and J(NC-γ) couplings. *J. Am. Chem. Soc.*, **119**, 1803–1804.

Ingham,K.C., Brew,S.A. and Atha,D.H. (1990) Interaction of heparin with fibronectin and isolated fibronectin domains. *Biochem. J.*, **272**, 605–611.

Jacob,K., Bosserhoff,A.K., Wach,F., Knuchel,R., Klein,E.C., Hein,R. and Buettner,R. (1995) Characterization of selected strongly and weakly invasive sublines of a primary human melanoma cell line and isolation of subtractive cDNA clones. *Int. J. Cancer*, **60**, 668–675.

Jahnke,W., Baur,M., Gemmecker,G. and Kessler,H. (1995) Improved accuracy of NMR structures by a modified NOESY-HSQC experiment. *J. Magn. Reson.*, **106**, 86–88.

Jones,J.A., Hodgkinson,P., Barker,A.L. and Hore,P.J. (1996) Optimal sampling strategies for the measurement of spin-spin relaxation times. *J. Magn. Reson. B*, **113**, 25–34.

Kelley,L.A., MacCallum,R.M. and Sternberg,M.J.E. (2000) Enhanced genome annotation using structural profiles in the program 3D-PSSM. *J. Mol. Biol.*, **299**, 499–520.

Klaus,W., Broger,C., Gerber,P. and Senn,H. (1993) Determination of the disulphide bonding pattern in proteins by local and global analysis of nuclear magnetic resonance data. Application to flavoridin. *J. Mol. Biol.*, **232**, 897–906.

Koch,C.A., Anderson,D., Moran,M.F., Ellis,C. and Pawson,T. (1991) SH2 and SH3 domains: elements that control interactions of cytoplasmic signaling proteins. *Science*, **252**, 668–674.

Koradi,R., Billeter,M. and Wüthrich,K. (1996) MOLMOL: a program for display and analysis of macromolecular structures. *J. Mol. Graph.*, **14**, 51–55.

Lakowicz,J.R. (1983) *Principles of Fluorescence Spectroscopy*. Plenum Press, New York, NY.

Lippens,G., Dhalluin,C. and Wieruszeski,J.M. (1995) NOE spectroscopy, water suppression, and water flip-back. Use of a water flip-back pulse in the homonuclear NOESY experiment. *J. Biomol. NMR*, **5**, 327–331.

Marion,D., Ikura,M., Tschudin,R. and Bax,A. (1989a) Rapid recording of 2D NMR-spectra without phase cycling—application to the study of hydrogen-exchange in proteins. *J. Magn. Reson.*, **85**, 393–399.

Marion,D., Driscoll,P.C., Kay,L.E., Wingfield,P.T., Bax,A., Gronenborn,A.M. and Clore,G.M. (1989b) Overcoming the overlap problem in the assignment of ^1H NMR spectra of larger proteins by use of three-dimensional heteronuclear ^1H-^{15}N Hartman-Hahn-multiple quantum coherence and nuclear Overhauser-multiple quantum coherence spectroscopy: application to interleukin 1β. *Biochemistry*, **28**, 6150–6156.

Martínez,J.C. and Serrano,L. (1999) The folding transition state between SH3 domains is conformationally restricted and evolutionarily conserved. *Nature Struct. Biol.*, **6**, 1010–1016.

McAlister,M.S.B., Mott,H.R., van der Merwe,A., Campbell,I.D., Davis,S.J. and Driscoll,P.C. (1996) NMR analysis of interacting

soluble forms of the cell–cell recognition molecules CD2 and CD48. *Biochemistry*, **35**, 5982–5991.

McCarthy,J.B., Chelberg,M.K., Mickelson,D.J. and Furcht,L.T. (1988) Localization and chemical synthesis of fibronectin peptides with melanoma adhesion and heparin binding activities. *Biochemistry*, **27**, 1380–1388.

Mohri,H., Katoh,K., Iwamatsu,A. and Okubo,T. (1996a) The novel recognition site in the C-terminal heparin-binding domain of fibronectin by integrin $\alpha_4\beta_1$ receptor on HL-60 cells. *Exp. Cell Res.*, **222**, 326–332.

Mohri,H., Tanabe,J., Katoh,K. and Okubo,T. (1996b) Identification of a novel binding site to the integrin $\alpha_{IIb}\beta_3$ located in the C-terminal heparin-binding domain of human plasma fibronectin. *J. Biol. Chem.*, **271**, 15724–15728.

Mongiovi,A.M., Romano,P.R., Panni,S., Mendoza,M., Wong,W.T., Musacchio,A., Cesareni,G. and Di Fiore,P.P. (1999) A novel peptide–SH3 interaction. *EMBO J.*, **18**, 5300–5309.

Mori,S., Abeygunawardana,C., Johnson,M.O. and Vanzijl,P.C.M. (1995) Improved sensitivity of HSQC spectra of exchanging protons at short interscan delays using a new fast HSQC (FHSQC) detection scheme that avoids water saturation. *J. Magn. Reson.*, **108**, 94–98.

Mould,A.P. and Humphries,M.J. (1991) Identification of a novel recognition sequence for the integrin $\alpha_4\beta_1$ in the COOH-terminal heparin-binding domain of fibronectin. *EMBO J.*, **10**, 4089–4095.

Mould,A.P., Askari,J.A., Craig,S.E., Garatt,A.N., Clements,J. and Humphries,M.J. (1994) Integrin $\alpha_4\beta_1$-mediated melanoma cell adhesion and migration on vascular cell adhesion molecule-1 (VCAM-1) and the alternatively spliced IIICS region of fibronectin. *J. Biol. Chem.*, **269**, 27224–27230.

Movilla,N. and Bustelo,X.R. (1999) Biological and regulatory properties of Vav-3, a new member of the vav family of oncoproteins. *Mol. Cell. Biol.*, **19**, 7870–7885.

Mühlhahn,P. *et al*. (1998) Structure of interleukin 16 resembles a PDZ domain with an occluded peptide binding site. *Nature Struct. Biol.*, **5**, 682–686.

Müller-Ladner,U., Bosserhoff,A.K., Dreher,K., Hein,R., Neidhart,M., Gay,S., Scholmerich,J., Buettner,R. and Lang,B. (1999) MIA (melanoma inhibitory activity): a potential serum marker for rheumatoid arthritis. *Rheumatology*, **38**, 148–154.

Musacchio,A., Saraste,M. and Wilmanns M. (1994) High-resolution crystal structures of tyrosine kinase SH3 domains complexed with proline-rich peptides. *Nature Struct. Biol.*, **1**, 546–551.

Potts,J.R. and Campbell,I.D. (1994) Fibronectin structure and assembly. *Curr. Opin. Cell Biol.*, **6**, 648–655.

Rance,M., Sorensen,O.W., Bodenhausen,G., Wagner,G., Ernst,R.R. and Wuthrich,K. (1983) Improved spectral resolution in COSY ^{1}H-NMR spectra of proteins via double quantum filtering. *Biochem. Biophys. Res. Commun.*, **117**, 479–485.

Renner,C. and Holak,T.A. (2000) Separation of anisotropy and exchange broadening using ^{15}N CSA-^{15}N-^{1}H dipole-dipole relaxation cross-correlation experiments. *J. Magn. Reson.*, **145**, 192–200.

Riddle,D.S., Grantcharova,V.P., Santiago,J.V., Alm,E., Ruczinski,I. and Baker,D. (1999) Experiment and theory highlight role of native state topology in SH3 folding. *Nature Struct. Biol.*, **6**, 1016–1024.

Schultz,J., Copley,R.R., Doerks,T., Ponting,C.P. and Bork,P. (2000) SMART: a web-based tool for the study of genetically mobile domains. *Nucleic Acids Res.*, **28**, 231–234.

Shaka,A.J., Lee,C.J. and Pines,A. (1988) Iterative schemes for bilinear operators—application to spin decoupling. *J. Magn. Reson.*, **77**, 274–293.

Sharma,A., Askari,J.A., Humphries,M.J., Jones,E.Y. and Stuart,D.I. (1999) Crystal structure of a heparin- and integrin-binding segment of human fibronectin. *EMBO J.*, **18**, 1468–1479.

Shuker,S.B., Hajduk,P.J., Meadows,R.P. and Fesik,S.W. (1996) Discovering high-affinity ligands for proteins: SAR by NMR. *Science*, **274**, 1531–1534.

Sklenar,V., Piotto,M., Leppik,R. and Saudek,V. (1993) Gradient-tailored water suppression for ^{1}H-^{15}N HSQC experiments optimized to retain full sensitivity. *J. Magn. Reson.*, **102**, 241–245.

Stoll,R., Voelter,W. and Holak,T.A. (1997) Conformation of thymosin β_9 in water/fluoroalcohol solution determined by NMR spectroscopy. *Biopolymers*, **41**, 623–634.

Stoll,R. *et al.* (2000) Letter to the Editor: Sequence-specific ^{1}H, ^{13}C, and ^{15}N assignment of the human melanoma inhibitory activity (MIA) protein. *J. Biomol. NMR*, **17**, 91–92.

Talluri,S. and Wagner,G. (1996) An optimized 3D NOESY-HSQC. *J. Magn. Reson.*, **112**, 200–205.

Tessari,M.F., Mulder,A.A., Boelens,R. and Vuister,G.W. (1997) Determination of amide proton CSA in ^{15}N-labeled proteins using ^{1}H CSA/^{15}N-^{1}H dipolar and ^{15}N CSA/^{15}N-^{1}H dipolar cross-correlation rates. *J. Magn. Reson.*, **127**, 128–133.

Van Groningen,J.J.M., Bloemers,H.P. and Swart,G.W. (1995) Identification of melanoma inhibitory activity and other differentially expressed messenger RNAs in human melanoma cell lines with different metastatic capacity by messenger RNA differential display. *Cancer Res.*, **55**, 6237–6243.

Vuister,G.W. and Bax,A. (1993) Quantitative *J* correlation—a new approach for measuring homonuclear 3-bond J(H(N)H(α)) coupling-constants in ^{15}N-enriched proteins. *J. Am. Chem. Soc.*, **115**, 7772–7777.

Wishart,D.S., Sykes,B.D. and Richards,F.M. (1991) Relationship between nuclear magnetic shift and protein secondary structure. *J. Mol. Biol.*, **222**, 311–333.

Wüthrich,K. (1986) *NMR of Proteins and Nucleic Acids*. John Wiley & Sons, New York, NY.

Yu,H., Rosen,M.K., Shin,T.B., Seidel-Dugan,C., Brugge,J.S. and Schreiber,S.L. (1992) Solution structure of the SH3 domain of Src and identification of its ligand binding site. *Science*, **258**, 1665–1668.

Yu,H., Chen,J.K., Feng,S., Dalgarno,D.C., Brauer,A.W. and Schreiber,S.L. (1994) Structural basis for the binding of proline-rich peptides to SH3 domains. *Cell*, **76**, 933–945.

Received July 7, 2000; revised December 11, 2000; accepted December 12, 2000